Supporting Information

Photochemical and Electrocatalytic Water Oxidation with Cobalt Carbodiimide (CoNCN)

Debora Ressnig, Menny Shalom, Jörg Patscheider, René Moré, Fabio Evangelisti, Markus Antonietti and Greta R. Patzke**

Table of contents

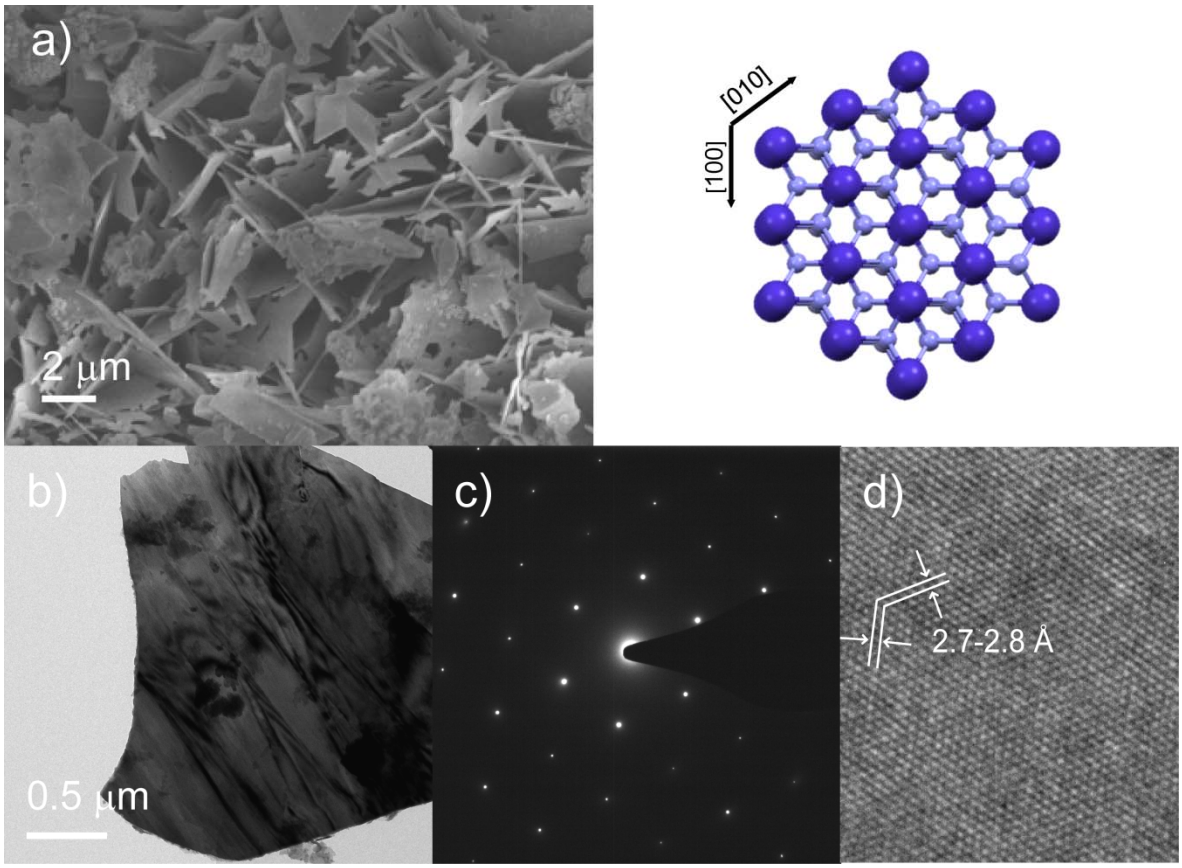

Figure S1. (a) Representative SEM image and (b) TEM micrograph of CoNCN platelets; (c) the corresponding SAED pattern (001 zone axis) displays high crystallinity and outlines the hexagonal packing of Co atoms in the (002) plane; (d) HRTEM of CoNCN (observed spacing corresponds to the stacking distance $d_{(100)}$ of CoNCN (ICDD 04-015-1039)).

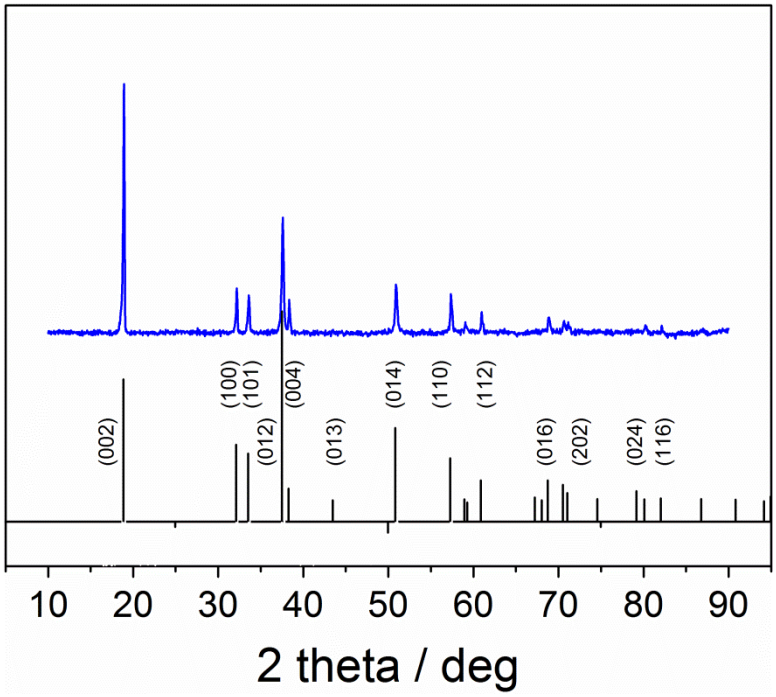

***Figure S2*.** PXRD pattern of CoNCN vs. reference data (ICDD 04-015-1039).

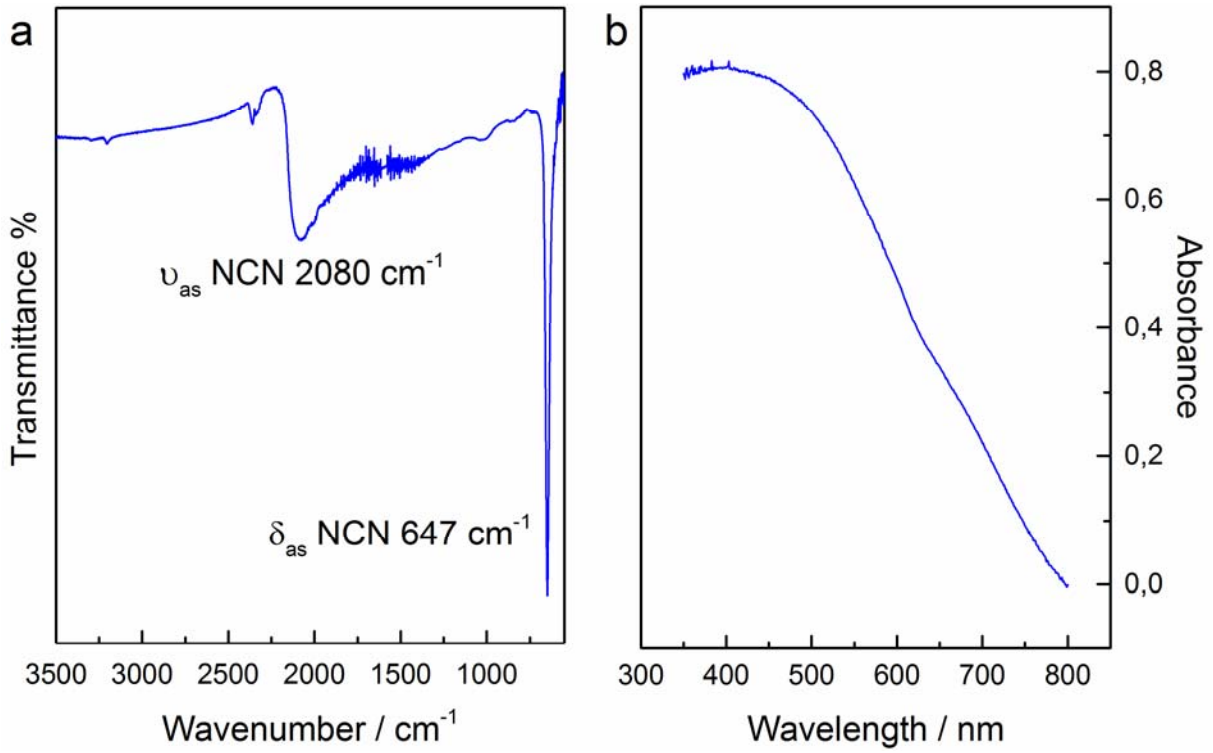

***Figure S3*.** (a) FTIR spectrum of CoNCN, (b) UV/vis spectrum of CoNCN.

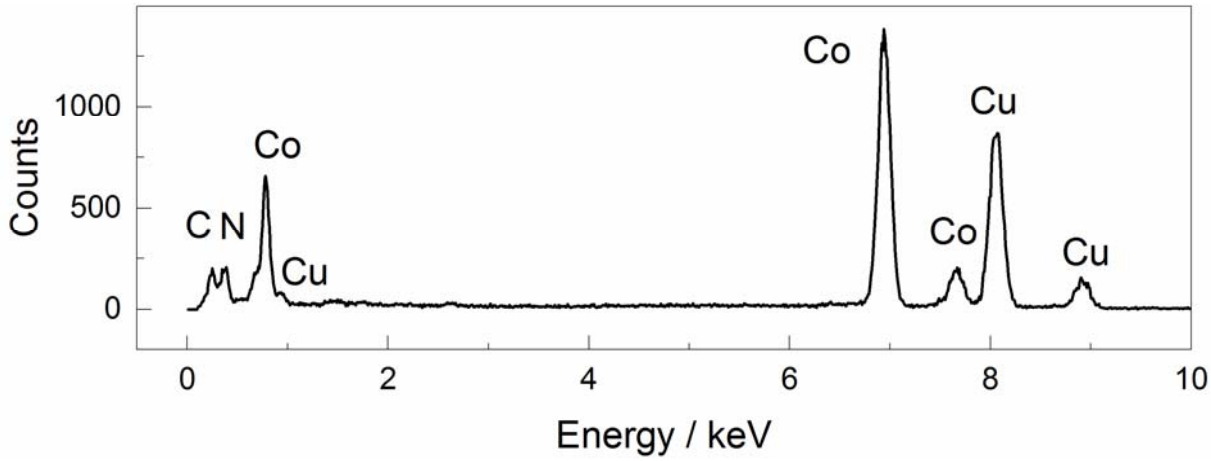

***Figure S4*.** Representative EDX spectrum of CoNCN deposited on a copper grid.

Table S1. Elemental analysis data of CoNCN.

CoNCN	N	C	H
Determined	30	12	<1
Calculated	28	12	-

Table S2. Water oxidation activity of various CoNCN concentrations under standard photocatalytic conditions (1 mM $[Ru(bpy)_3]^{2+}$, 5 mM $Na_2S_2O_8$, 470 nm, 8 mL buffer).

	pH	Buffer	Catalyst/ mM	O_2 yield[a]/ %	TOF/S_{BET}/ g s^{-1} m^{-2}
1	9	phosphate	5.0	16	3.8×10^{-2}
2	9	phosphate	2.5	31	1.0×10^{-1}
3	9	phosphate	1.5	73	1.4×10^{-1}
4	9	phosphate	1.0	46	1.7×10^{-1}
5	9	phosphate	0.5	18	1.3×10^{-1}
6	9	phosphate	0.2	12	1.3×10^{-1}
7	9	carbonate	1.5	76	2.1×10^{-1}
8	9	carbonate	1.2	55	1.9×10^{-1}
9	9	carbonate	0.8	46	1.4×10^{-1}
10	9	carbonate	0.4	10	5.2×10^{-2}
11	9	carbonate	0.2	3	2.1×10^{-2}
12	7	phosphate	1.5	18	1.3×10^{-2}
13	8	phosphate	1.5	19	8.5×10^{-2}
14	9	phosphate	1.5	73	1.4×10^{-1}
15	9	carbonate	1.5	76	2.1×10^{-1}
16	9	borate	1.5	50	1.5×10^{-1}

[a]Oxygen produced relative to the initial $Na_2S_2O_4$ amount: 2 $[O_2]$/ $[Na_2S_2O_4]$

Table S3. Reference experiments for CoNCN under different catalytic conditions (1 mM $[Ru(bpy)_3]Cl_2$ PS, 5 mM $Na_2S_2O_8$ and 1.5 mM of catalyst in carbonate buffer pH 9).

Catalyst	Electron acceptor	PS	Irradiation	OER activity
-	$S_2O_8^{2-}$	-	Yes	No
-	-	$[Ru(bpy)_3]^{2+}$	Yes	No
-	$S_2O_8^{2-}$	$[Ru(bpy)_3]^{2+}$	No	No
CoNCN	-	-	Yes	No
CoNCN	$S_2O_8^{2-}$	-	Yes	No
CoNCN	-	$[Ru(bpy)_3]^{2+}$	Yes	No
CoNCN	$S_2O_8^{2-}$	$[Ru(bpy)_3]^{2+}$	No	No
CoNCN	$S_2O_8^{2-}$	$[Ru(bpy)_3]^{2+}$	Yes	**Yes**

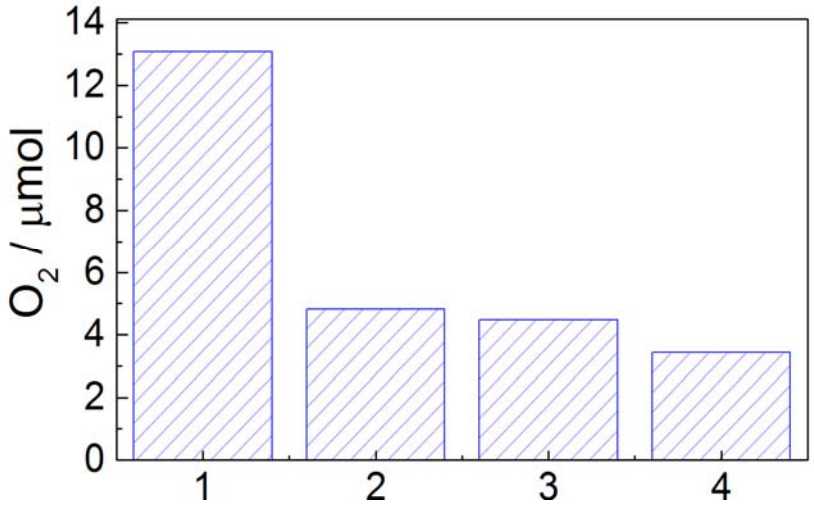

***Figure S5*.** Absolute amounts of oxygen produced in recycling experiments with CoNCN (2.5 mM) under standard conditions (1 mM $[Ru(bpy)_3]^{2+}$, 5 mM $Na_2S_2O_8$, 470 nm, gas chromatography analysis). After each run, the catalyst was collected by centrifugation and immersed in a fresh aqueous solution of PS and electron acceptor.

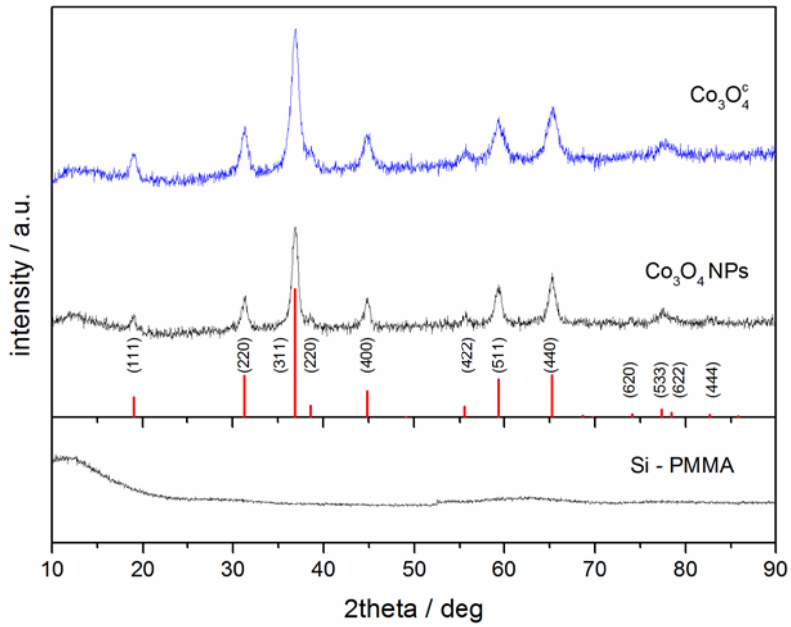

Figure S6. PXRD patterns of hydrothermally synthesized nanoparticles and commercially purchased Co_3O_4 catalysts (reference: ICDD 04-007-8056).

Patterns were recorded on a Si-PMMA sample holder. The untreated raw data, as shown here, indicate the nanocrystalline character of the materials and the absence of significant background scattering from amorphous Co_3O_4 powders.

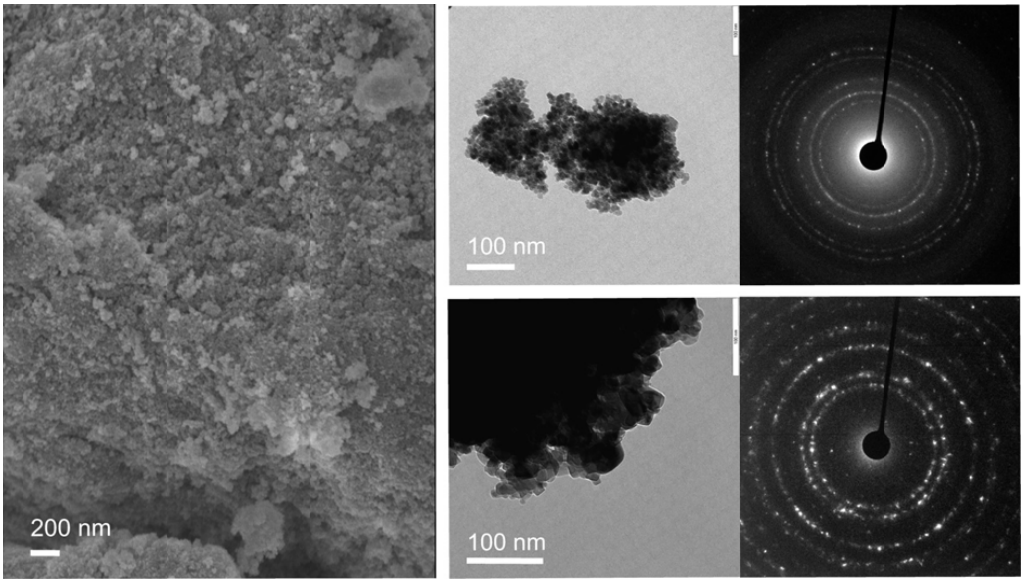

Figure S7. Representative SEM (left), TEM (middle) and SAED (right) images of hydrothermally synthesized Co_3O_4 nanoparticles.

SAED patterns indicate that the particles are phase pure, e.g. in agreement with the PXRD patterns shown in Figure S6.

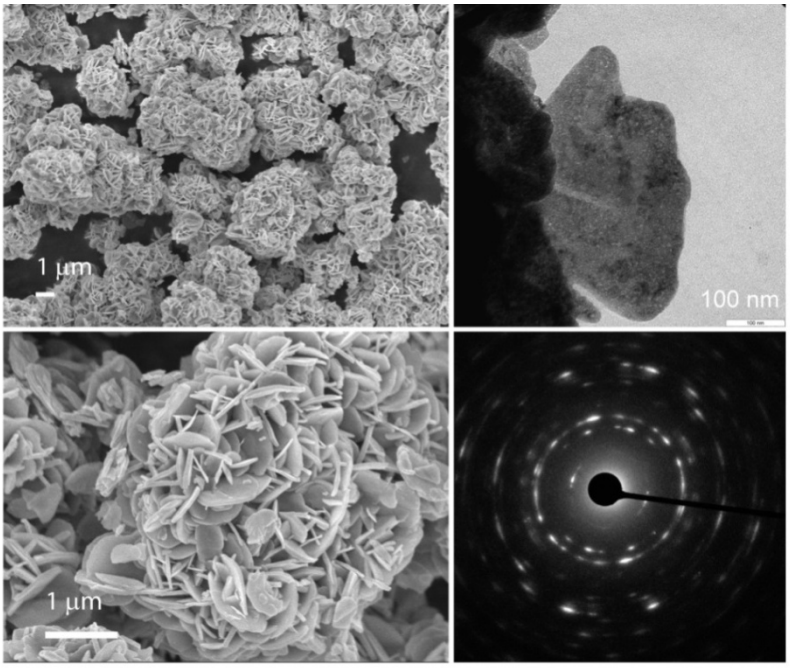

Figure S8. Representative SEM and TEM images of commercially purchased Co_3O_4 powders.

The corresponding SAED pattern (bottom right) is consistent with the characteristics of a multicrystalline material and shows no significant amorphous background (cf. PXRD pattern shown in Figure S7).

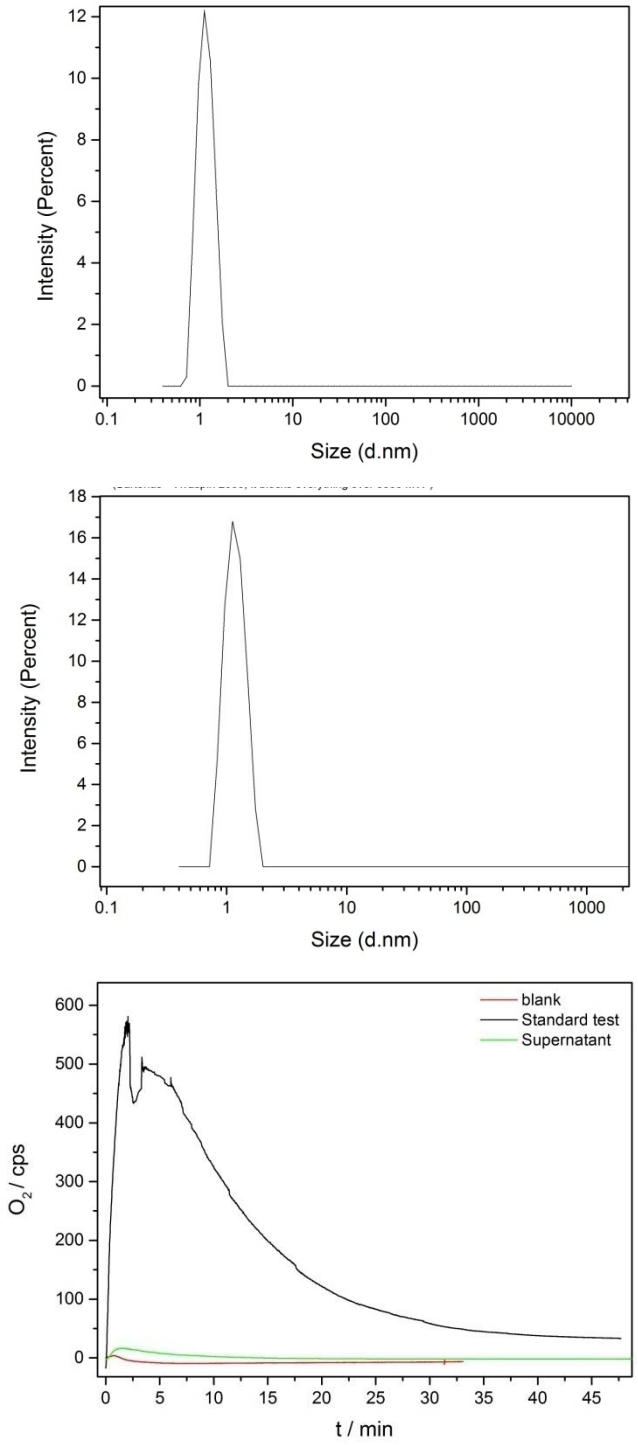

Figure S9. Dynamic light scattering (DLS) characterization of pure water (*top*, reference experiment) and of the supernatant solution recovered after catalysis (*middle*; recovered by centrifugation) and (*bottom*) Clark electrode kinetics of visible-light-driven O_2 evolution for (1) standard test (black; conditions: 1.2 mM CoNCN, 470 nm LED, 1 mM $[Ru(bpy)_3]Cl_2$, 5 mM $Na_2S_2O_8$, pH 9 (carbonate buffer)), (2) blank test (red; absence of CoNCN) and (3) recycling test of the supernatant solution (green; post-catalytic supernatant solution was recovered by centrifugation and 5 mM $Na_2S_2O_8$ and 1 mM $[Ru(bpy)_3]Cl_2$ were newly added).

Control experiments to exclude RuO_2 as a catalytically active species were performed by replacing CoNCN with Ru-containing test compounds (RuO_2 (MW: 133 g/mol) and $RuCl_3 \cdot xH_2O$ (MW: 207.43 g/mol)).

Ru contents were adjusted to simulate an overall degradation of the photosensitizer (1 mM $[Ru(bpy)_3]Cl_2$) that could give rise the formation of an equimolar amount of RuO_2 (1 mM). Furthermore, a lower extent (10%) of PS decomposition was modeled using 0.1 mM RuO_2. Parallel tests were performed replacing RuO_2 with $RuCl_3 \cdot xH_2O$ under equivalent conditions.

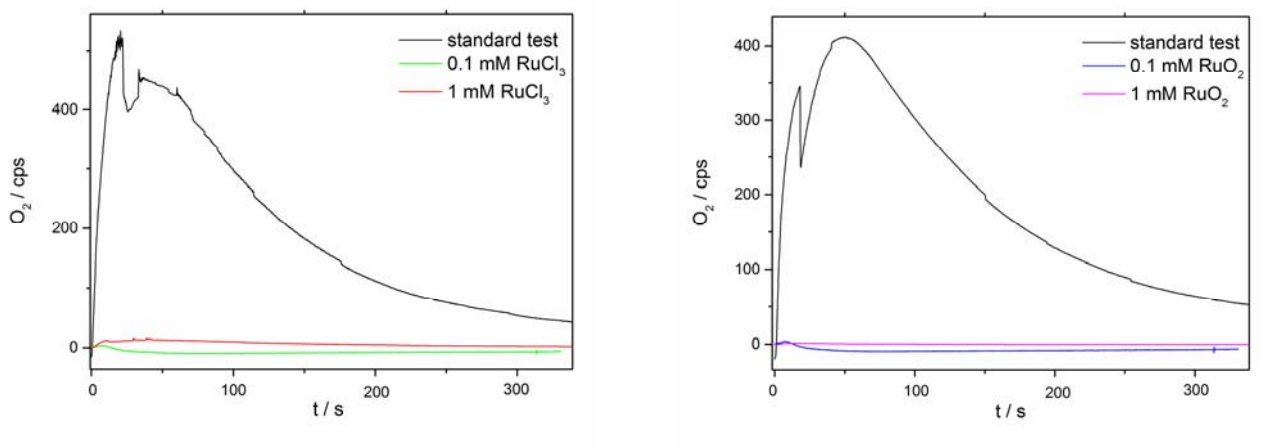

Figure S10. Clark-electrode kinetics of visible-light-driven O_2 evolution for representative WOC tests with 1.5 mM CoNCN catalyst compared to: replacement of CoNCN with 0.1-1 mM RuO_2 (left) and replacement of CoNCN with 0.1-1 mM of $RuCl_3 \cdot xH_2O$ (right; conditions: 470 nm LED; 1 mM $[Ru(bpy)_3]Cl_2$, 5 mM $Na_2S_2O_8$, pH 9 (carbonate buffer)) excluding a 10%-100% degradation of $[Ru(bpy)_3]Cl_2$ as a source of oxide-based WOCs.

The reaction dispersions were prepared under dark conditions by adding the corresponding amounts of CoNCN catalysts, 1 mM $[Ru(bpy)_3]Cl_2$ (5.94 mg) and 5 mM of $Na_2S_2O_8$ to 8 mL of DI H_2O in a glass vessel which was subsequently sealed. Control experiments were performed in different buffer solutions (0.4 M phosphate, 0.1 M carbonate and 0.5 M borate), all yielding no significant WOC activity.

Experimental: Cyanide determination in CoNCN suspensions

Three 0.1 M solutions of CoNCN (1 mL, carbonate buffer, Table S4: entries 4 - 6) were prepared for cyanide determination as described below together with three 0.1 M solutions of CoNCN and 9.52 mg of $Na_2S_2O_8$ (1 mL carbonate buffer, entries 5 - 7). Reference tests were conducted with 0.1 M buffer solutions of NaCN (1 mL, entries 1 - 3) at different concentrations.

Table S4. Cyanide determination for CoNCN with NaCN reference experiments.

Exp.	mg NaCN
1	0.2
2	0.1
3	0.05

Exp.	mg CoNCN
4	2.4
5	1.34
6	0.72

Exp.	mg CoNCN
5	2.4
6	1.34
7	0.72

The solutions containing all reagents were shaken in an agitator (Biosan Thermo-Shaker TS-100) for 44 h, followed by centrifugation for 20 min at 12.000 rpm to ensure removal of any suspended particles. Colorimetric detection tests[1-3] of CN^- with diaquacobinamide ($(H_2O)_2Cbi^{2+}$) were carried out with the obtained supernatant solutions.

All reference NaCN tests provided positive results in optical cyanide detection.
In contrast, all tests results including CoNCN were negative, showing the absence of significant CN^- concentrations (above 0.0023 M) in CoNCN suspensions, also in the presence of sodium persulfate. This clearly demonstrates that CoNCN is stable against cyanide leaching under the given conditions.

[1] C. Männel-Croisé, F. Zelder, *Inorg. Chem*. **2009**, *48*, 1272.
[2] C. Männel-Croisé, B. Probst, F. Zelder, *Anal. Chem*. **2009**, *81*, 9493.
[3] J. Ma, P. G. Dasgupta, F. H. Zelder, G. R. Boss, *Anal. Chim. Acta* **2012**, *736*, 78.

Determination of cyanamide and hydrolysis products in supernatant media

CoNCN (30 mg) was aged for 24 h in pure water, carbonate buffer (pH 9), carbonate buffer with $[Ru(bpy)_3]^{2+}$ and $S_2O_8^{2-}$ and as post catalytic suspension with constant stirring. The supernatant was removed by high speed centrifugation and subsequently passed through Millipore-filters (200 nm) to remove CoNCN. Water was removed by lyophilization and the solid residues were analyzed with FT-IR spectroscopy.

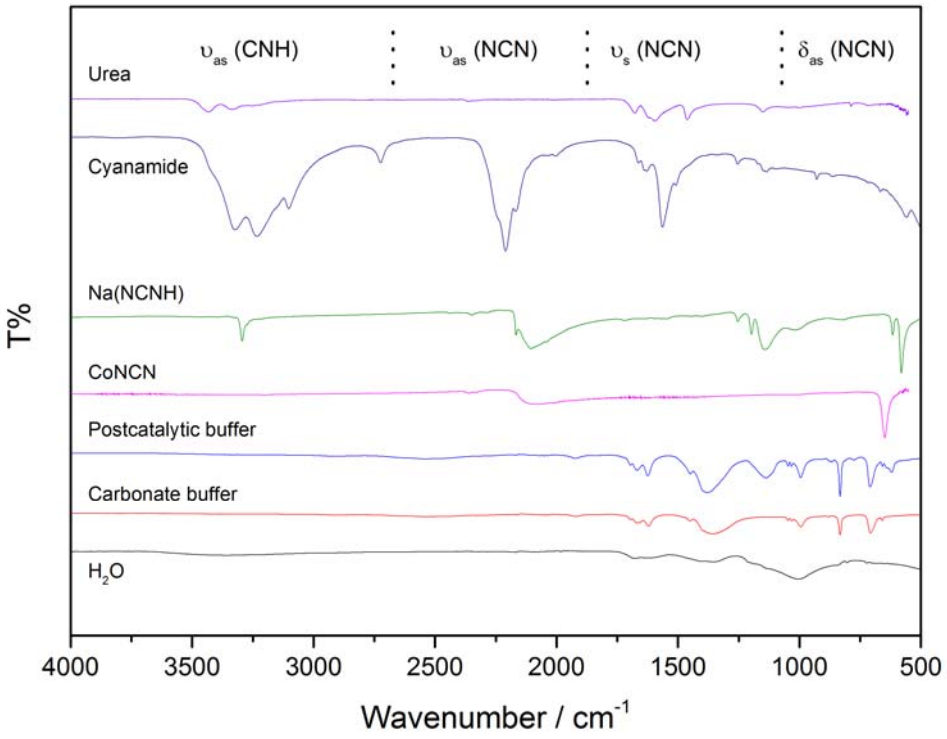

Figure S11. FT-IR spectra of CoNCN samples aged in different solutions. Comparison to reference spectra of different cyanamide derivatives and absence of characteristic absorption frequencies provides strong evidence for the absence of NCN^{2-} leaching products.

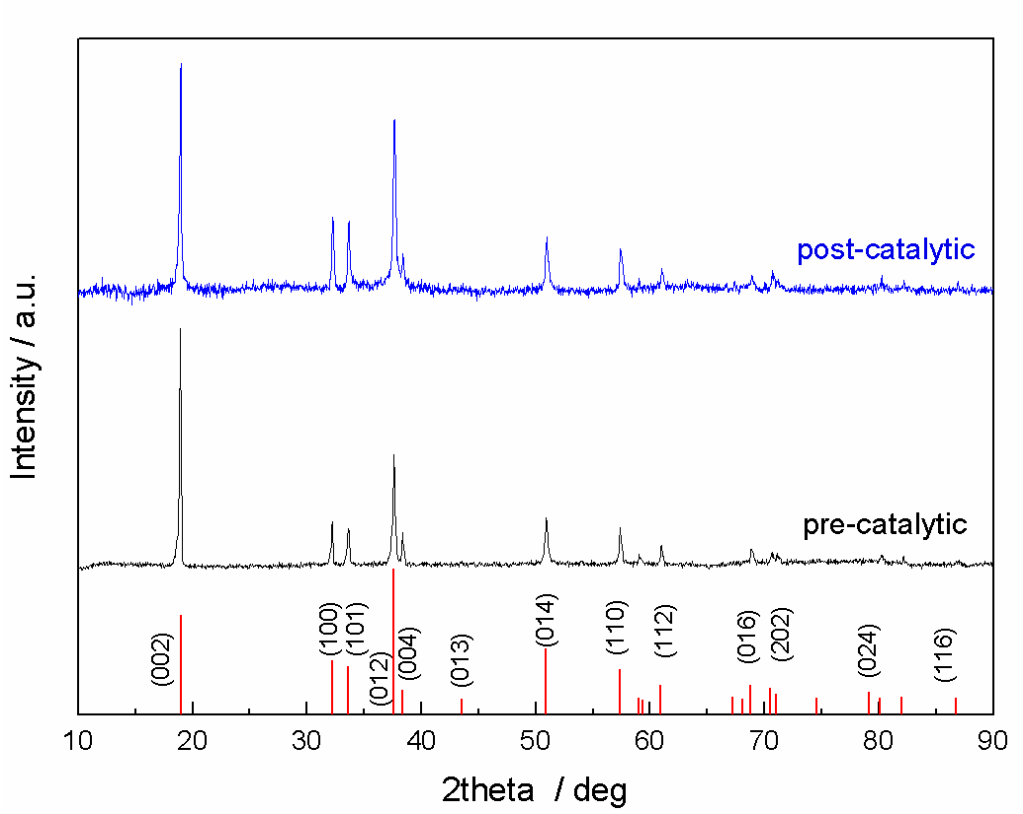

***Figure S12*.** PXRD patterns of CoNCN before (black) and after photocatalysis (blue) in carbonate buffer at pH 9 (reference pattern: ICDD 04-015-1039).

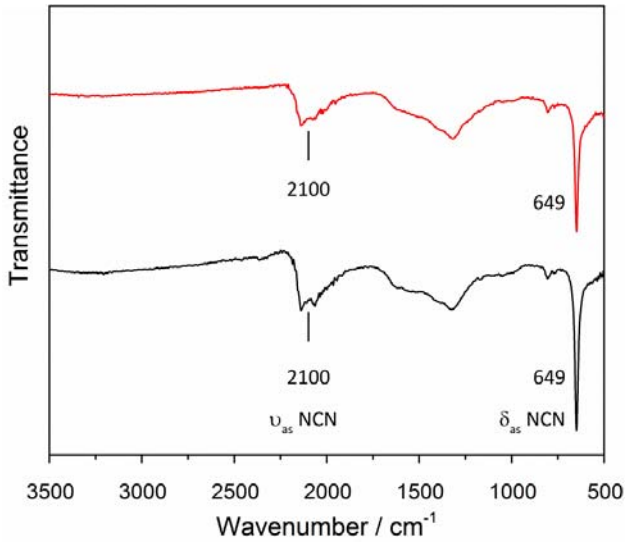

***Figure S13*.** FT-IR spectra of CoNCN before (black) and after photocatalysis (red) in carbonate buffer (pH 9). The broad band between 1600 cm^{-1} and 1200 cm^{-1} corresponds to the side product melem.

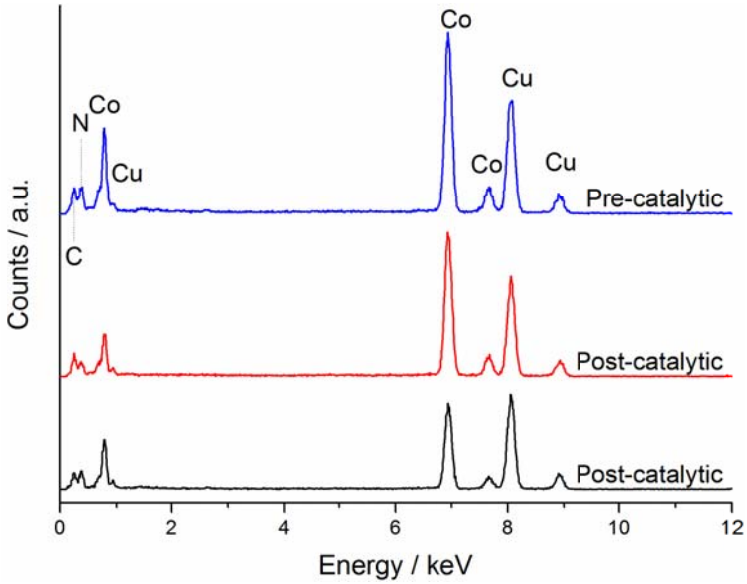

Figure S14. Representative EDX spectra of pristine (blue) and post-catalytic CoNCN (red, black; recorded on copper grids).

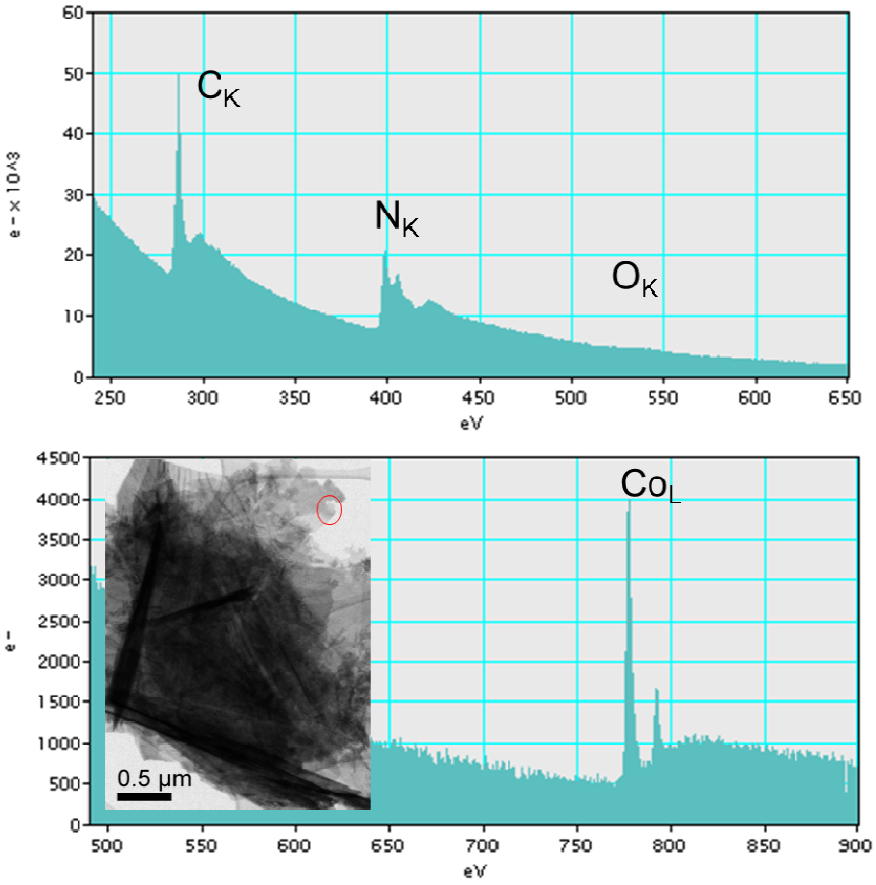

Figure S15. Representative electron energy loss spectrum of CoNCN after photocatalytic experiments at pH 9 with typical carbodiimide features at the N_K and C_K– edge.[4]

[4] O. Lichtenberger, J. Woltersdorf, N. Hering, R. Riedel, *Z. Anorg. Allg. Chem.* **2000**, *626*, 1881.

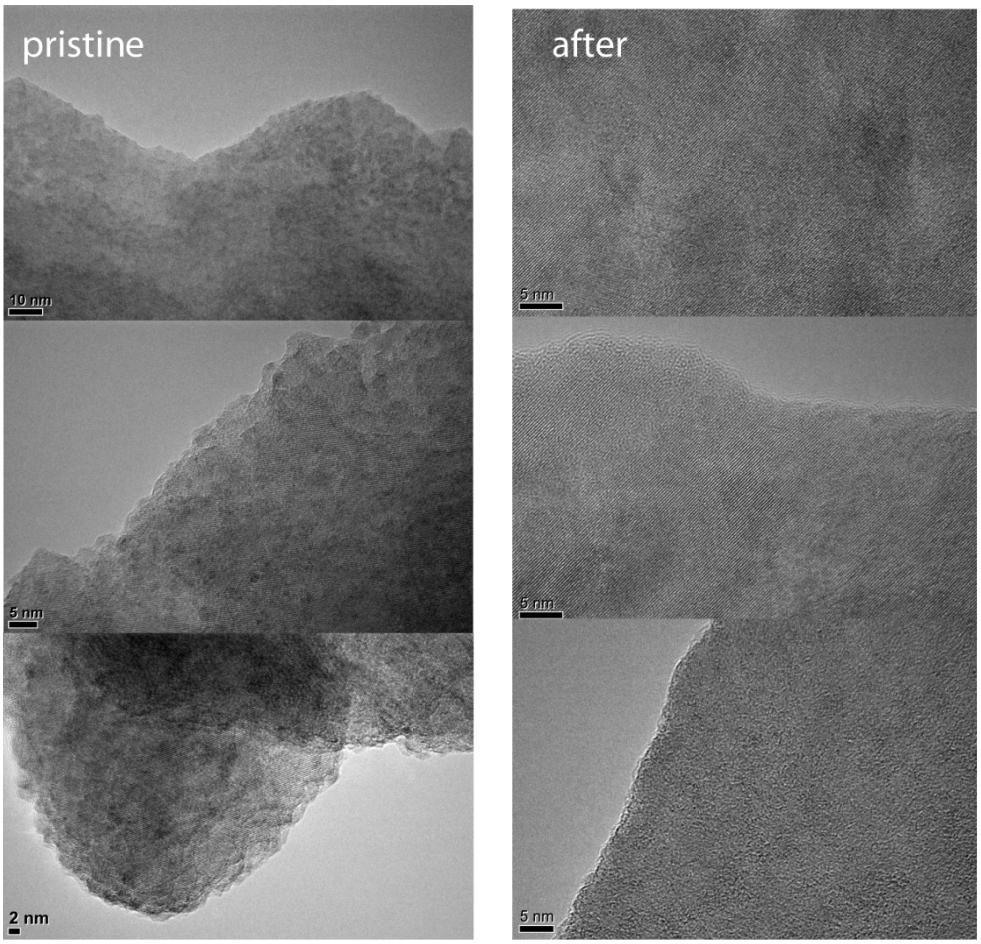

Figure S16. Representative HRTEM images of CoNCN WOC before and after photocatalysis in carbonate buffered solution (pH 9).

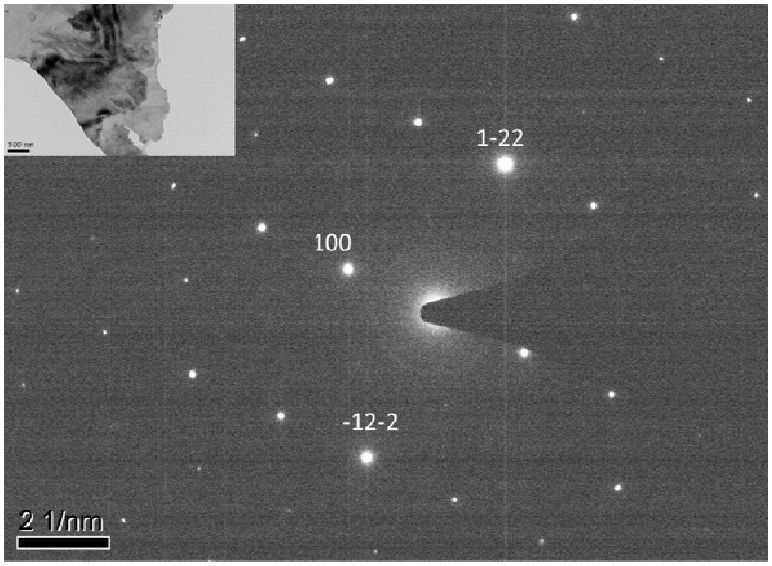

Figure S17. SAED pattern of the [001] zone axis of post-catalytic (pH 9) CoNCN.

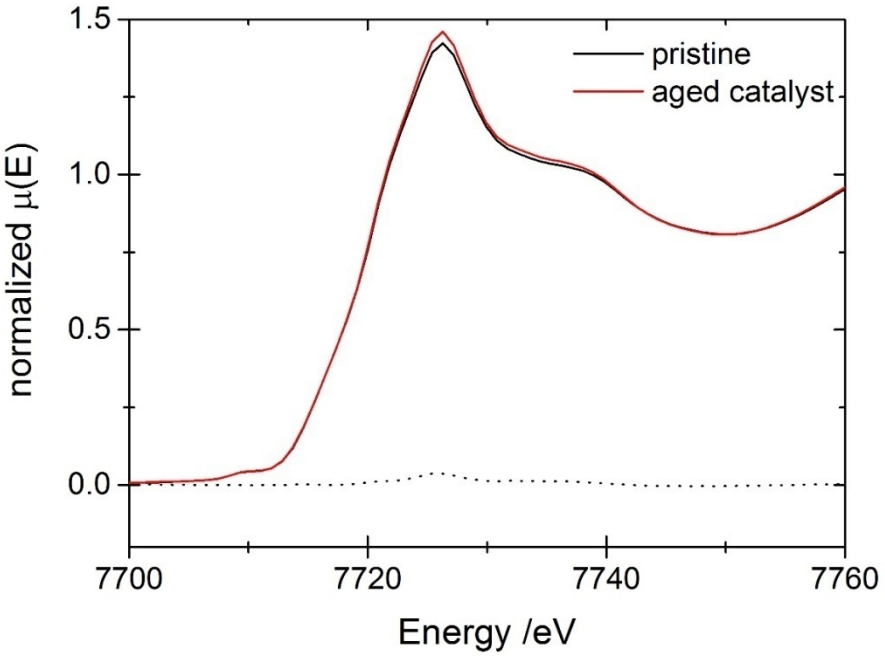

Figure S18. XANES region for pristine and in carbonate buffer (pH 9) aged CoNCN and their difference spectrum.

Table S5. EXAFS fit results for pristine and post-catalytic CoNCN in comparison with crystallographic reference data (single crystal X-ray diffraction).

	pristine CoNCN		**post-catalytic CoNCN**		**scXRD[5]**
	r/Å	**σ^2/Å^2**	**r/Å**	**σ^2/Å^2**	**r/Å**
Co N1	2.15±0.01	$(9\pm2)\cdot10^{-3}$	2.11±0.01	$(12\pm2)\cdot10^{-3}$	2.168
C1	2.96±0.01	$(9\pm2)\cdot10^{-3}$	2.91±0.02	$(12\pm2)\cdot10^{-3}$	2.992
Co2	3.21±0.01	$(10\pm1)\cdot10^{-3}$	3.20±0.02	$(16\pm2)\cdot10^{-3}$	3.213
N2	3.84±0.02	$(9\pm2)\cdot10^{-3}$	3.76±0.02	$(3\pm2)\cdot10^{-2}$	3.876

[5] M. Krott, X. Liu, Xiaohui, B. P. T. Fokwa, M. Speldrich, H. Lueken, R. Dronskowski, *Inorg. Chem*. **2007**, *46*, 2204.

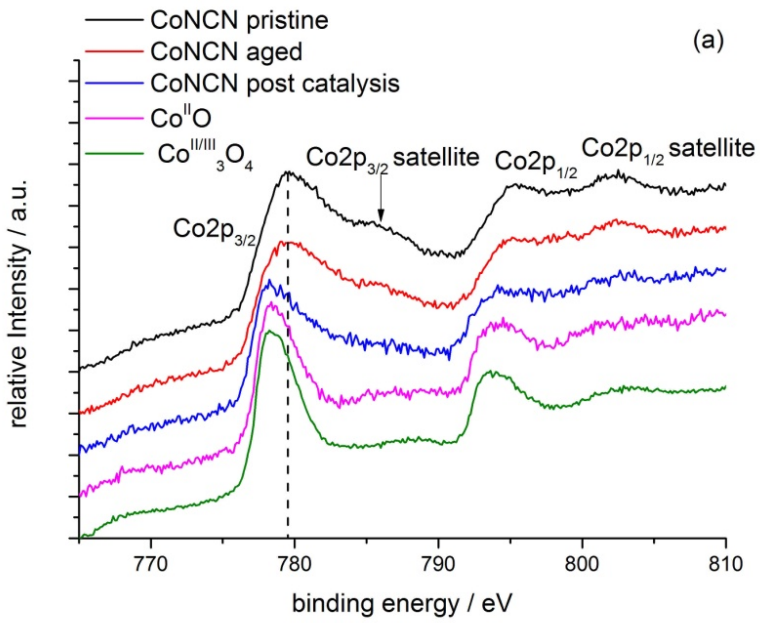

Figure S19. XPS analysis of CoNCN (pristine, aged in carbonate buffer and post-photocatalytic) vs. oxide references: (a) Co2p XPS peaks, (b) O1s XPS peaks.

Three CoNCN sample types were subjected to XPS and EXAFS/XANES analyses in order to verify the integrity of the photocatalyst in catalytic media and after the water oxidation process: (1) pristine CoNCN, (2) CoNCN aged in buffer solution and (3) post-catalytic CoNCN.
In line with the XANES results (see main text), no significant differences were found for the Co2p XPS peak positions of pristine, aged and post-catalytic CoNCN which would clearly point to the presence of significant Co^{3+} after the photocatalytic process. The Co2p peak positions of Co^{2+}/Co^{3+} are generally very close and difficult to distinguish, and the observed differences for the CoNCN samples fall within the +/- 1 eV deviation range reported in various reference studies.[6, 7] This is evident from the virtually identical Co2p$_{3/2}$ peak positions of Co(II)O (778.3 eV) and Co(II,III)$_3$O$_4$ (778.2 eV). Furthermore, the rather low spectral resolution of the untreated CoNCN samples did not permit an according data fit.

[6] N. S. McIntyre, M. G. Cook, *Anal. Chem*. **1975**, *47*, 2208.

[7] M. C. Biesinger, B. P. Payne, A. P. Grosvenor, L. W. M. Lau, A. R. Gerson, R. St. C. Smart, *Appl. Surf. Sci.* **2011**, *257*, 2717.

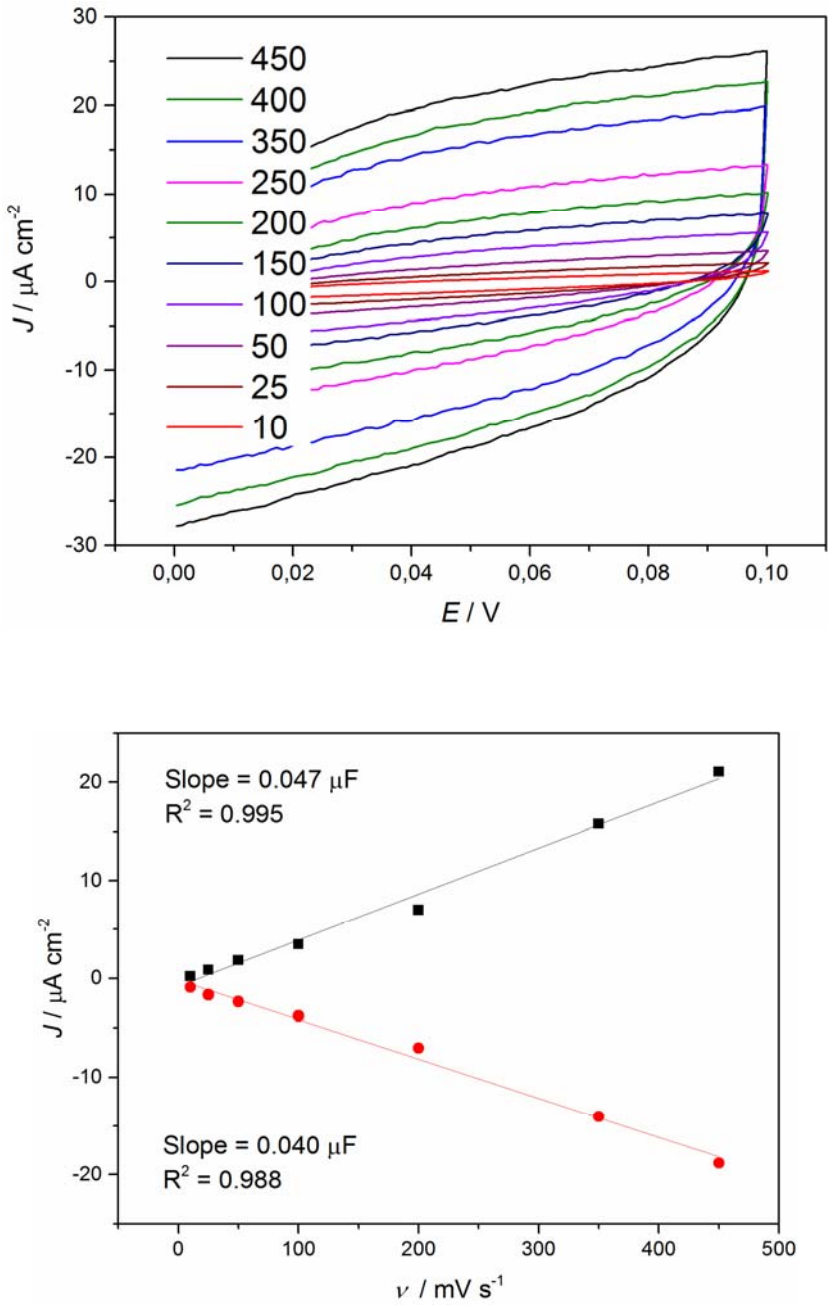

Figure S20. Cyclovoltammograms of the CoNCN electrode recorded in the non-Faradaic region (0 - 0.1 V) at various rates (10 – 450 mV s^{-1}) in 0.1 M phosphate buffer (pH 6.9).

The electrode was held at each potential for 10s before the measurement. The electrochemical double layer capacitance C_{DL} was extracted from $i_c = \nu C_{DL}$, where ν is the scan rate and i_c the current density for the specific curve at 0.05 mV. The evaluation indicates low capacitive current in line with the LSV measurements in the manuscript Figure 5 and with the microcrystalline structure of the catalysts.

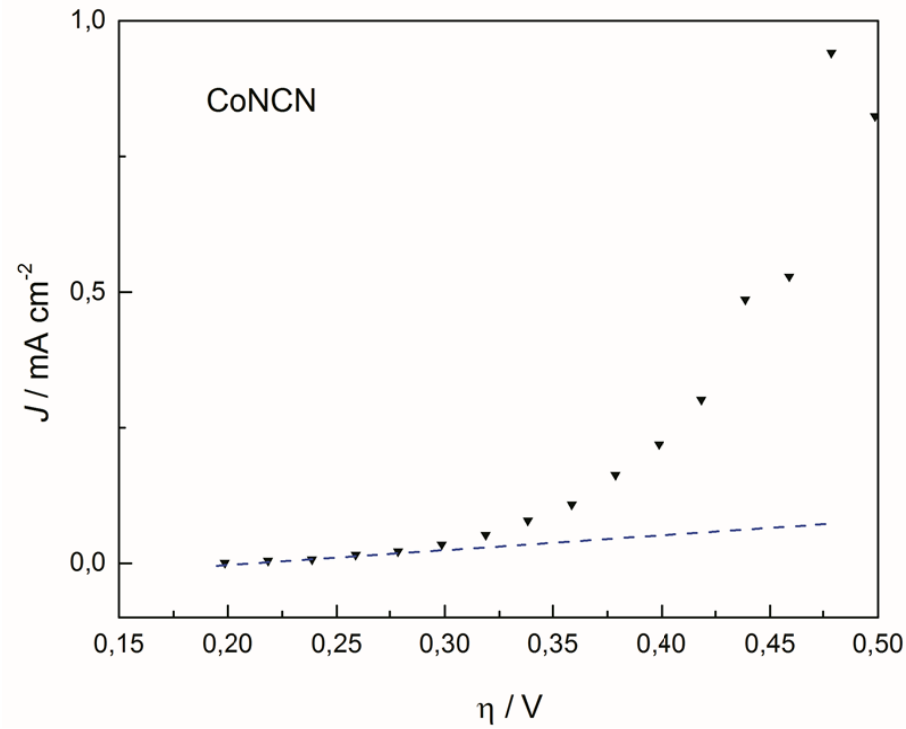

Figure S21. Current density obtained with CoNCN in the water oxidation onset region. Data points were collected by chronoamperometry measurements with 60 s equilibrium time in 0.1 M phosphate buffer (pH 6.9).

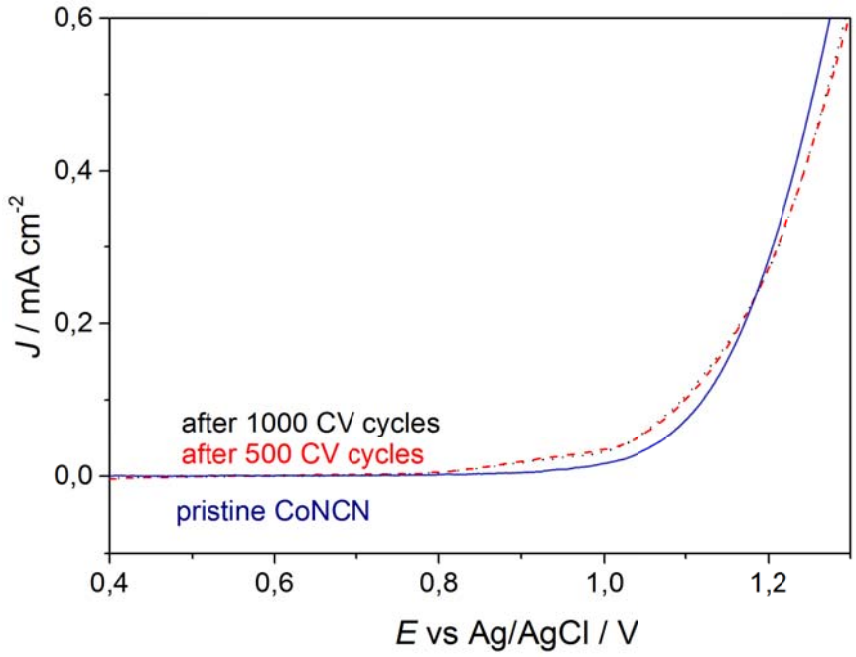

Figure 22. LSV curves of CoNCN were recorded before cyclic voltammetry measurements, after 500 and 1000 cycles under standard conditions (glassy carbon electrodes, 0.1 M phosphate buffer at pH 7, scan rates: CV 100 mV s^{-1}, LSV 1 mV s^{-1}, 1500 rpm). 1/3 of the usual amounts of CoNCN was deposited on the electrode to minimize rotation induced material losses in the measurement.

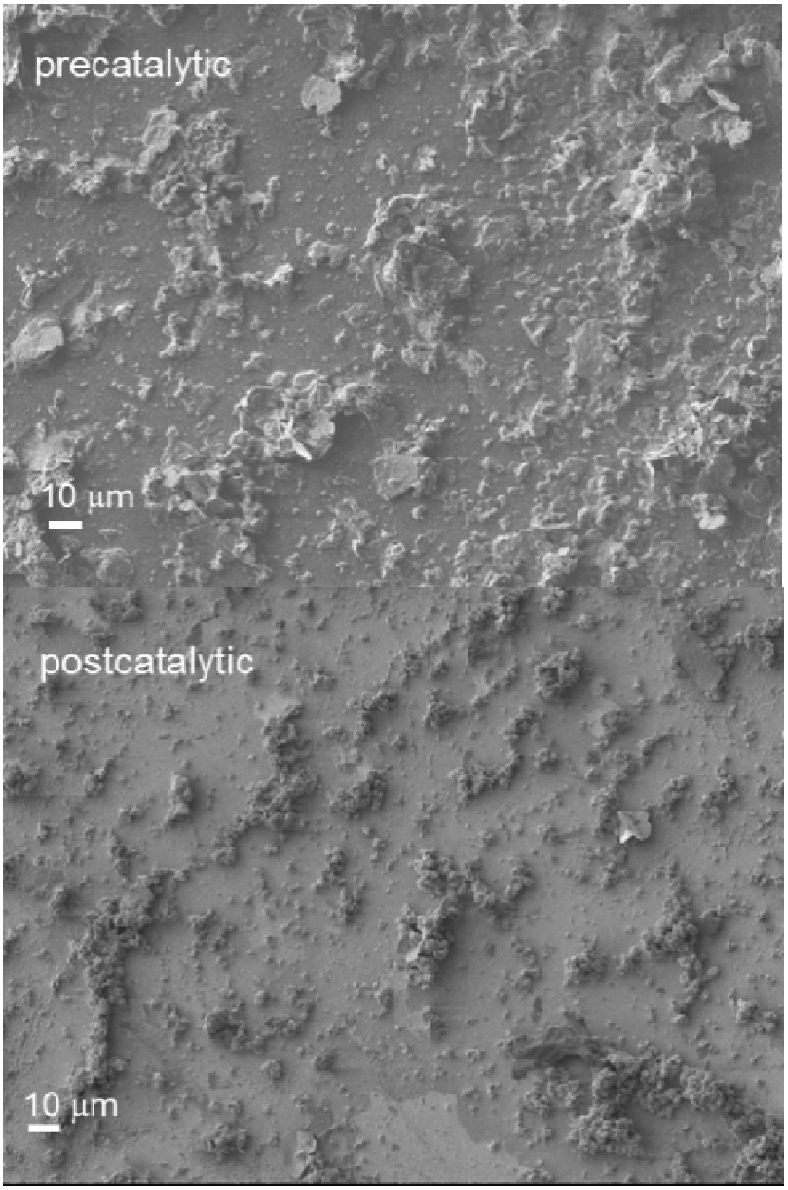

Figure S23. Representative SEM images of FTO glass electrodes before and after the stability tests.

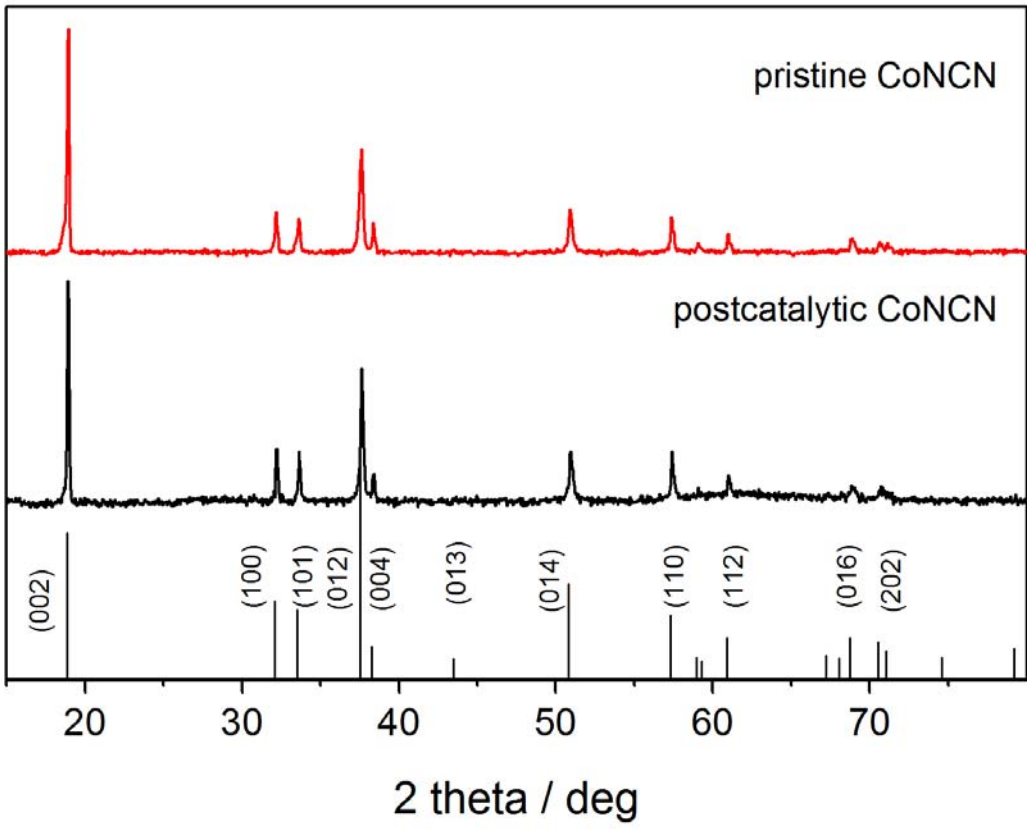

Figure S24. PXRD patterns of CoNCN before (red) and after electrocatalytic experiments (black) in phosphate buffered solution (pH 6.9). The catalyst was removed from the FTO glass for the measurement (reference pattern: CoNCN [ICDD 04-015-1039]).

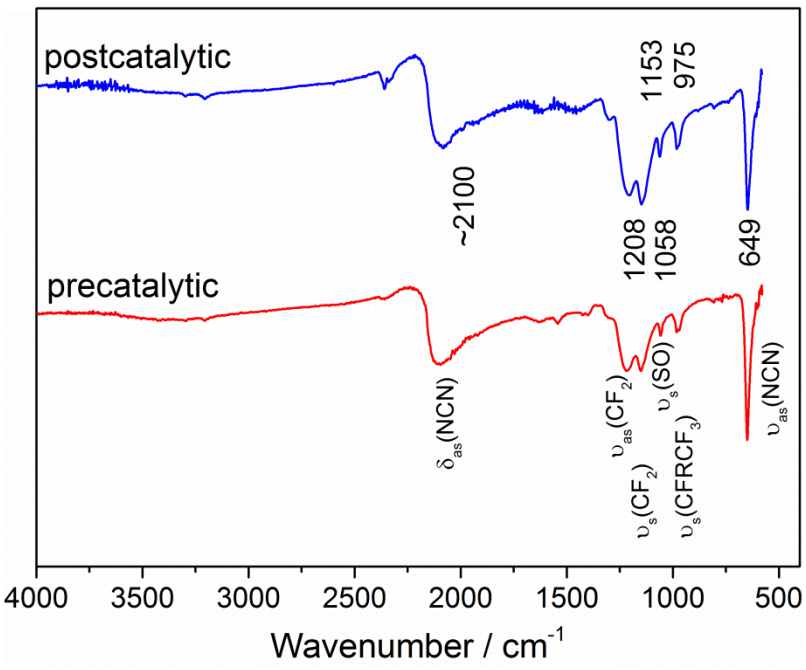

Figure S25. FT-IR spectra of CoNCN/Nafion mixtures before and after electrolysis

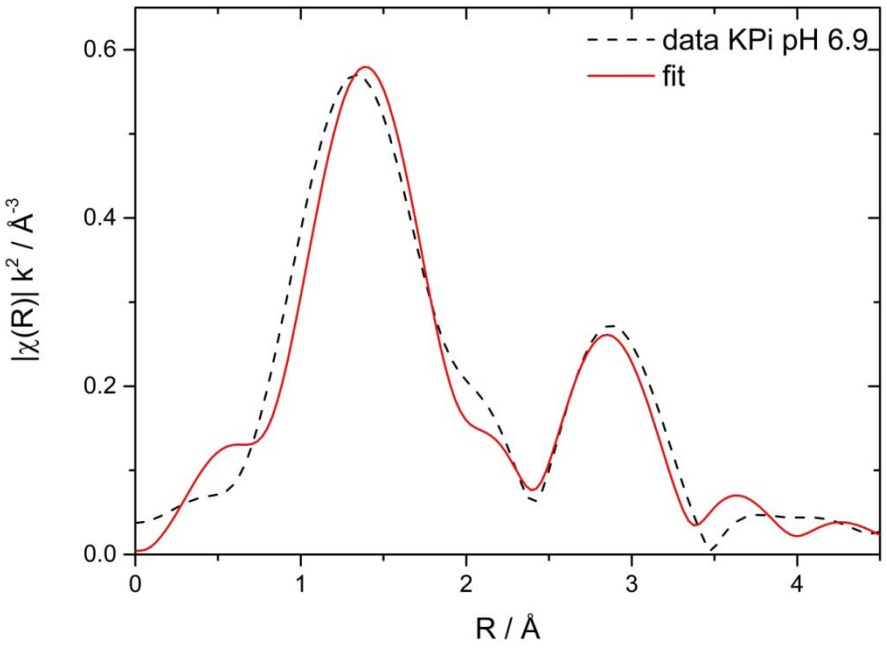

Figure S26. Representative EXAFS spectrum of CoNCN electrocatalyst on a FTO electrode after 20 h of electrolysis in KPi (pH 7) fitted vs. structural reference data.[5]

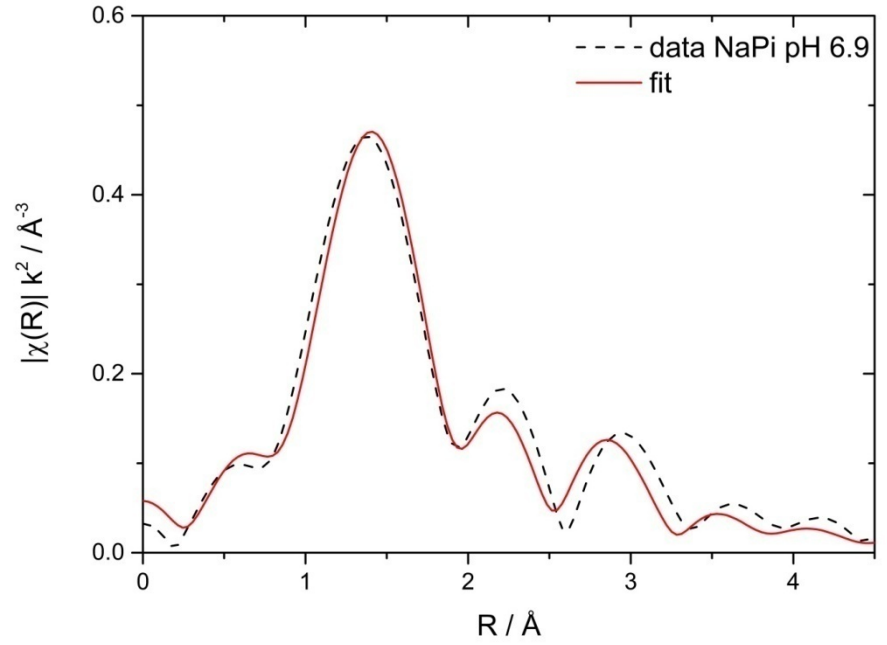

Figure S27. Representative EXAFS spectrum of CoNCN electrocatalyst on a FTO electrode after 20 h of electrolysis in NaPi (pH 7) fitted vs. structural reference data.[5]

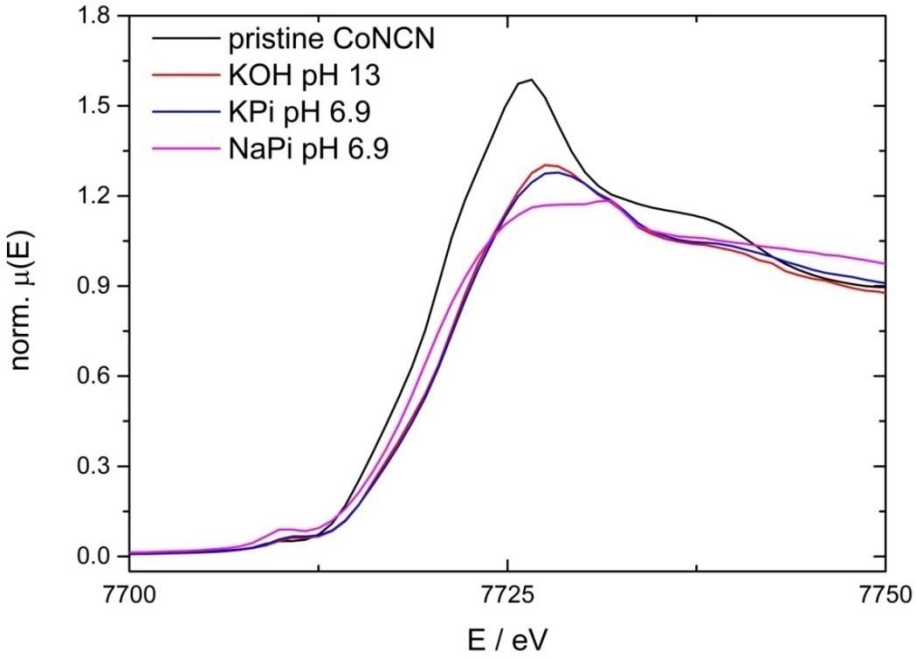

Figure S28. Representative XANES spectra of CoNCN electrocatalysts on FTO electrodes after 20 h of electrolysis in different media (KOH, NaPi, KPi) vs. reference data for pristine CoNCN.

Table S6. Linear combination fits for the XANES region of CoNCN electrocatalysts on FTO electrodes after 20 h of electrolysis in different media (KOH, NaPi, KPi).

electrode	redχ^2	Co(III) / %	Co(II) / %
NaPi pH 6.9	0.00028	29±3	71±3
KPi pH 6.9	0.00025	29±3	71±3
KOH pH 13	0.00023	27±3	73±3

Table S7. EXAFS fits for CoNCN electrocatalysts on FTO electrodes after 20 h of electrolysis in different media (KOH, NaPi, KPi).

electrode	R-factor	r_{Co-N}/ Å	σ^2_{Co-N}/ Å^2	r_{Co-C}/ Å	σ^2_{Co-N}/ Å^2
NaPi pH 6.9	2.7 %	1.96±0.2	(5±3)·10^{-3}	2.70±0.2	(8±4)·10^{-3}
KPi pH 6.9	2.1 %		(10±4)·10^{-3}		(10±4)·10^{-3}
KOH pH 13	1.5 %	2.02±0.2	(12.3±0.8)·10^{-3}	2.79±0.2	(8±4)·10^{-3}

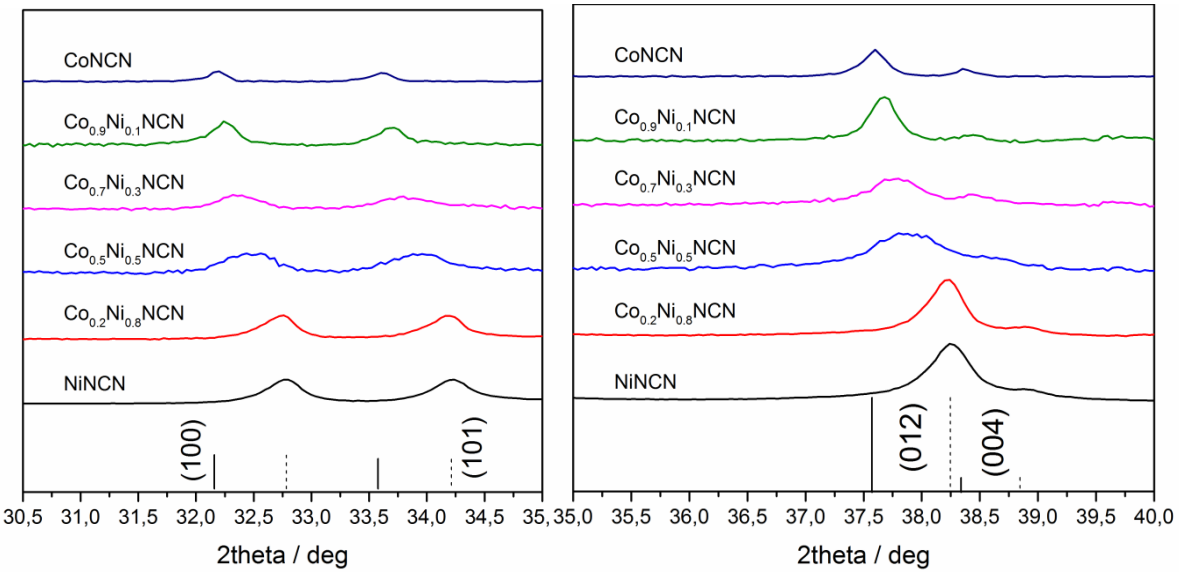

Figure S29. Magnification of the PXRD patterns of $Co_{1-x}Ni_xNCN$ catalysts with peak shifts (reference patterns: ── CoNCN [ICDD 04-015-1039] and - - - NiNCN [ICDD 04-015-1038]).

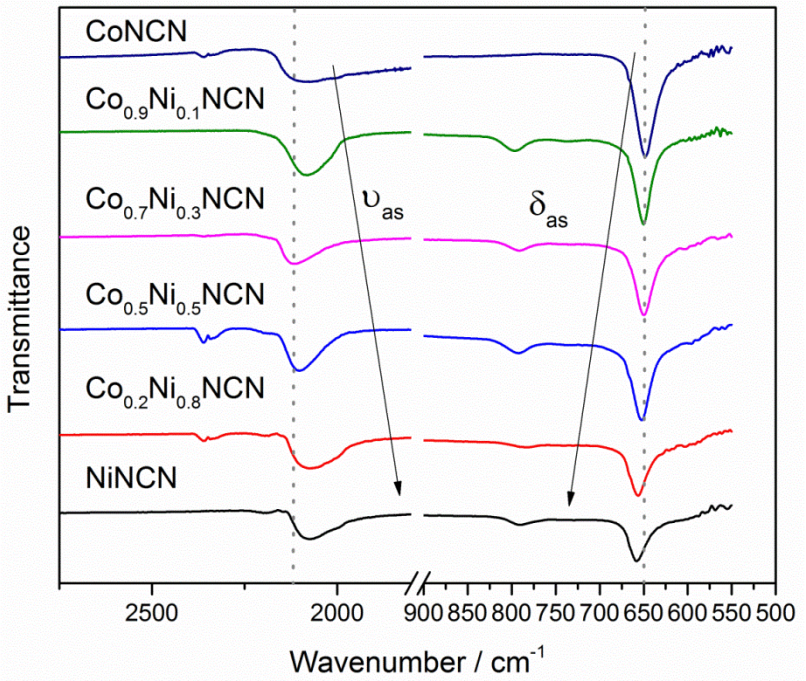

Figure S30. FT-IR spectra of $Co_{1-x}Ni_xNCN$ solid solutions depicting peak shifts of the asymmetric stretching and bending mode of the NCN^{2-} anion.

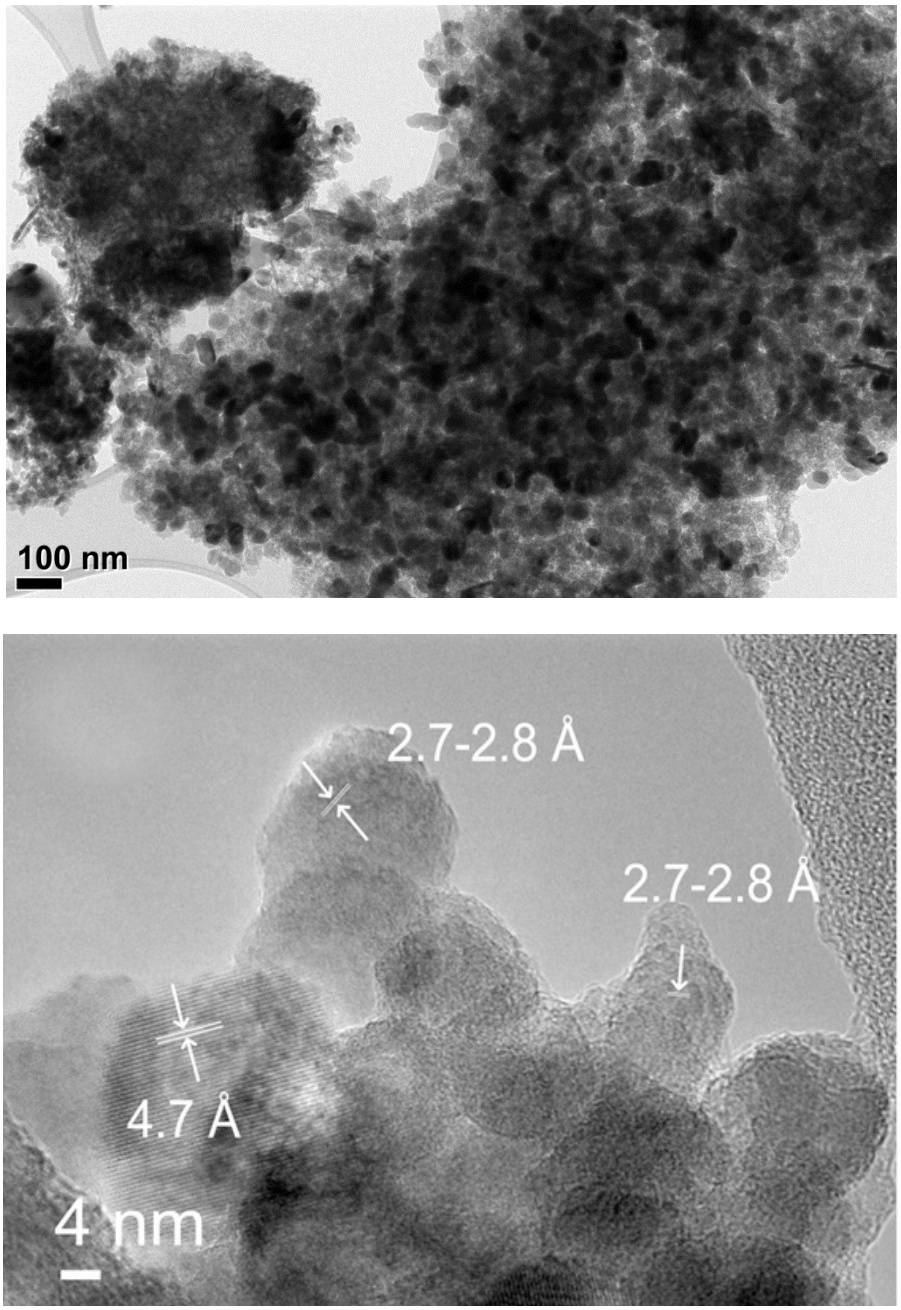

Figure S31. Representative(HR)TEM images of NiNCN powders (lattice fringes correspond well to the stacking distance $d_{(100)}$ of NiNCN [ICDD 04-015-1038]).

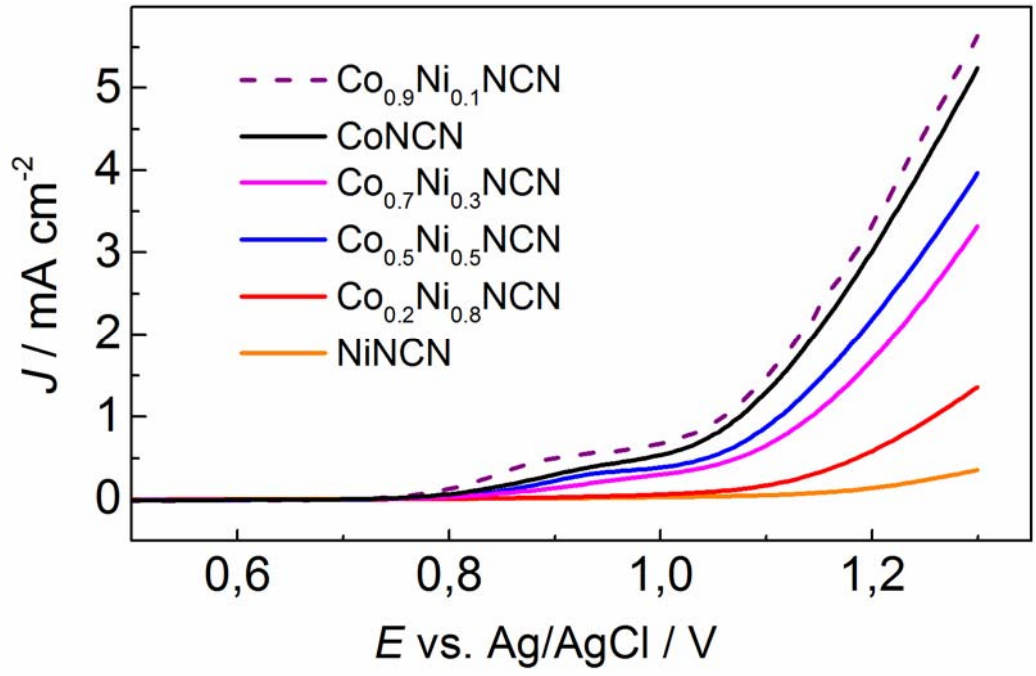

Figure S32. LSVs curves of $Co_{1-x}Ni_xNCN$ catalysts (glassy carbon electrodes, scan rate: 10 mV s^{-1}, 0.1 M phosphate buffer (pH 6.9)).